Quantum-enhanced estimation of the optical phase gradient by use of image-inversion interferometry

Walker Larson* and Bahaa E. A. Saleh

CREOL, The College of Optics and Photonics, University of Central Florida, 4304 Scorpius St, Orlando, Florida 32817, USA

(Received 31 March 2020; accepted 16 June 2020; published 13 July 2020)

We show that the quantum Cramér-Rao bound on the error of measurement of the optical phase gradient with a beam of finite width (or the wavefront tilt within a finite aperture) is consistent with the Fourier-transform uncertainty principle for the single-photon state, and is a factor of N lower for the maximally entangled N-photon state. This fundamental bound therefore governs the tradeoff between quantum sensitivity and spatial resolution. Error bounds for a structured configuration using binary projective-field measurements implemented by an image-inversion (II) interferometer are higher, and the factor of N advantage attained by the N-photon maximally entangled state is reduced and eventually washed out as the beam width or the phase gradient increases. This reduction is more rapid for larger N, so that the quantum advantage is more vulnerable. The precision of the II interferometer is greater than that based on a split detector placed in the focal plane of a lens.

DOI: 10.1103/PhysRevA.102.013712

I. INTRODUCTION

The performance of classical optical metrology is limited by standard classical limits on the precision of measurement of optical phase and amplitude. Quantum metrology uses optical probes in nonclassical states of light, enabling precision superseding those classical limits; nonetheless, new superior limits emerge as the ultimate quantum limits. For example, the standard quantum limit for estimation of the optical phase with an average of N photons is $1/\sqrt{N}$ [1], when the ultimate precision limit for a fixed number of photons N (Heisenberg quantum limit) is $1/N$ [2–6]. In this paper, we determine the quantum limit on the precision of measurement of the optical phase gradient, which is manifested by a local tilt of the optical wavefront within a finite aperture, or the angle of deflection of an optical beam of finite width introduced upon transmission through a thin slab with a spatially varying refractive index. We consider single-photon and multiphoton entangled quantum states and determine quantum Cramér-Rao (QCR) precision bounds based on the quantum Fisher information (QFI) [3,7–13]. As expected, these limits are inversely proportional to the beam width, in accord with the Fourier-transform uncertainty principle [14] and its generalization to a spatially coded two-photon state [15–17] that probes the phase slope in a manner similar to that of states used in NOON-state interferometry [18–21].

Specific measurement configurations aim at reaching the precision limits set by the QFI, but do not always attain these ultimate limits. One evident configuration is to convert the beam tilt into beam displacement by use of an optical Fourier-transform imaging system [22], as is usually done in the Shack-Hartmann system used in adaptive optics [23]. Standard measurements of beam displacement employ a split detector measuring detected photons in each of its two halves. Earlier studies of precision limits on estimates of displacement show that such configuration falls short of the quantum optimal precision by a factor of $\sqrt{\pi/2} \approx 1.25$ [24,25]. Although strategies that address this shortfall have been demonstrated, their implementation involves heterodyning of the displaced beam with an independent local oscillator in a specific spatial mode.

We consider here an alternative configuration: an image-inversion (II) interferometer [26–29] that utilizes interference between the phase-modulated beam and a spatially inverted copy of itself, and detects projections of the even component of the optical field distribution in one output port and that of the odd component in the other port. The Fisher information (FI) for this configuration is greater than that of the split detector and attains the quantum optimal precision for small phase gradients or narrow beam widths for both single-photon and multiphoton state implementations. However, as we show in this paper, the quantum advantage is reduced and eventually washed out as the phase-gradient beam-width product increases, and this deterioration is more severe for larger N, so that the greater the quantum advantage, the more vulnerable it is to the beam width and tilt.

II. QUANTUM FISHER INFORMATION FOR SINGLE- AND N-PHOTON STATES

An optical beam probes a phase object that introduces a phase $\phi(x)$ in the plane orthogonal to the beam direction. The beam width is assumed sufficiently narrow so that $\phi(x) \approx \phi_0 + \theta x$, where $\phi_0 = \phi(0)$ and $\theta = \partial\phi/\partial x\,|_{x=0}$. The phase gradient θ is to be estimated by use of measurements on the transmitted beam. This study is also applicable to measurement of the direction of an optical wave within a finite aperture.

*larsonwd@knights.ucf.edu

If the quantum state of the light transmitted through the phase object is described by a pure state $|\psi\rangle$, then the QFI is [30]

$$F_Q(\theta) = 4(\langle\psi'|\psi'\rangle - |\langle\psi|\psi'\rangle|^2), \tag{1}$$

where ψ' refers to the derivative of ψ with respect to θ. The QCR bound on the variance of the estimate of θ is $\sigma_\theta^2 \geqslant 1/F_Q(\theta)$. In the context of repeating the measurement process with M identically prepared illumination states, the variance of estiamtes of θ becomes limited in principle by $\sigma_\theta^2 \geqslant 1/(MF_Q(\theta))$.

In this section, we determine $F_Q(\theta)$ and the associated error bound σ_θ for light in two cases: single-photon, which corresponds to the limit imposed on any classical state of light, and an N-photon pure quantum state, which corresponds to the limit achievable by any state of light that seeks to use entanglement to aid estimation.

A. Single-photon state

If the single-photon state is a pure quantum state $|\psi_0\rangle = \int dx\, \psi_0(x)|x\rangle$, where $\psi_0(x)$ is an arbitrary wave function normalized such that $\int dx\, |\psi_0(x)|^2 = 1$, then upon transmission through the phase object the state becomes

$$|\psi\rangle = \int dx\, e^{-i\theta x}\psi_0(x)|x\rangle. \tag{2}$$

Based on Eq. (1), the QFI is

$$F_Q^{(1)}(\theta) = 4\int dx\, x^2|\psi_0(x)|^2 - 4\left|\int dx\, x|\psi_0(x)|^2\right|^2. \tag{3}$$

If $\psi_0(x)$ is an even function, then the second term in (3) vanishes, and

$$F_Q^{(1)}(\theta) = 4\sigma_x^2, \tag{4}$$

where $\sigma_x^2 = \int dx\, x^2|\psi_0(x)|^2$ is the second moment of the probability density function $|\psi_0(x)|^2$ and σ_x is a measure of its width. The QCR bound on the variance of the estimate of θ is $\sigma_\theta^2 = 1/F_Q^{(1)}(\theta)$, so that

$$\sigma_\theta\sigma_x = \tfrac{1}{2}. \tag{5}$$

Because the phase gradient θ equals the transverse component q of the wave vector, this is simply an expression of the bound dictated by the Fourier-transform-based uncertainty principle $\sigma_x\sigma_q = \frac{1}{2}$.

B. N-photon state

An N-photon pure quantum state is described by the integral $|\psi_0\rangle = \int \mathbf{dx}\ \psi_0(\mathbf{x})|\mathbf{x}\rangle$, where $\mathbf{x} = x_1, x_2, \ldots, x_N$, $\mathbf{dx} = dx_1dx_2\ldots dx_N$, and $\psi_0(\mathbf{x})$ is an arbitrary N-photon wave function normalized such that $\int \mathbf{dx}\, |\psi_0(\mathbf{x})|^2 = 1$. Upon transmission through the phase object, the state becomes

$$|\psi\rangle = \int \mathbf{dx}\, \psi_0(\mathbf{x})e^{-i\theta(\Sigma_\mathbf{x})}|\mathbf{x}\rangle, \tag{6}$$

where $\Sigma_\mathbf{x} = \sum_{n=1}^N x_n$. Using Eq. (1), the QFI is

$$F_Q^{(N)}(\theta) = 4\int \mathbf{dx}(\Sigma_\mathbf{x})^2|\psi_0(\mathbf{x})|^2 - 4\left|\int \mathbf{dx}(\Sigma_\mathbf{x})|\psi_0(\mathbf{x})|^2\right|^2. \tag{7}$$

Assuming a maximally entangled state $\psi_0(\mathbf{x}) = f_0(x_1)\Pi_{n=2}^N\delta(x_1 - x_n)$, i.e.,

$$|\psi\rangle = \int dx\, f_0(x)e^{-iN\theta x}|x\rangle^{\otimes N}, \tag{8}$$

and if $f_0(x)$ is an even function, then the second term of Eq. (7) vanishes and the QFI for the N-photon state is

$$F_Q^{(N)}(\theta) = 4N^2\sigma_x^2 = N^2F_Q^{(1)}, \tag{9}$$

where $\sigma_x^2 = \int dx\ x^2|f_0(x)|^2$ is a measure of the width of $|f_0(x)|^2$. Therefore, the minimum uncertainty σ_θ of estimates of the phase-gradient satisfies the relation

$$\sigma_\theta\sigma_x = \frac{1}{2N}. \tag{10}$$

The bound for the spatially entangled N-photon uncertainty product is therefore smaller than that of the single-photon case by a factor of N, assuming equal widths of the functions $|\psi_0(x)|^2$ in the single-photon case and $|f_0(x)|^2$ in the N-photon case.

III. FISHER INFORMATION FOR SPECIAL MEASUREMENT CONFIGURATIONS

We now consider specific configurations for measuring the phase gradient and assess their optimal precision in comparison with the ultimate quantum bounds described by (9) and (10). As with the QCRB, choosing a specific measurement strategy leads to estimation variance that is bounded by $\sigma_\theta^2 \geqslant 1/F(\theta)$, where the Fisher information

$$F(\theta) = \sum_i \frac{1}{P_i}\left(\frac{dP_i}{d\theta}\right)^2, \tag{11}$$

and P_i is the probability of measuring experimental outcome i. As before, repeating the measurement with M identically prepared illumination states provides sensitivity $\sigma_\theta^2 \geqslant 1/(MF(\theta))$.

A. Split detector in focal plane

The split detector is a two-sided detector that measures the lateral displacement of an optical beam by detecting the optical power on each side. When a beam described by a symmetric optical field $\psi_f(x)$ is centered on the detector, the intensity $|\psi_f(x)|^2$ on each half will be equal and the difference of the photon counts will be zero, on average. This changes, however, if the beam is displaced by some distance s. The powers in the two detectors are then

$$\begin{aligned} P_+ &= \int_0^\infty dx\, |\psi_f(x-s)|^2, \\ P_- &= \int_{-\infty}^0 dx\, |\psi_f(x-s)|^2, \end{aligned} \tag{12}$$

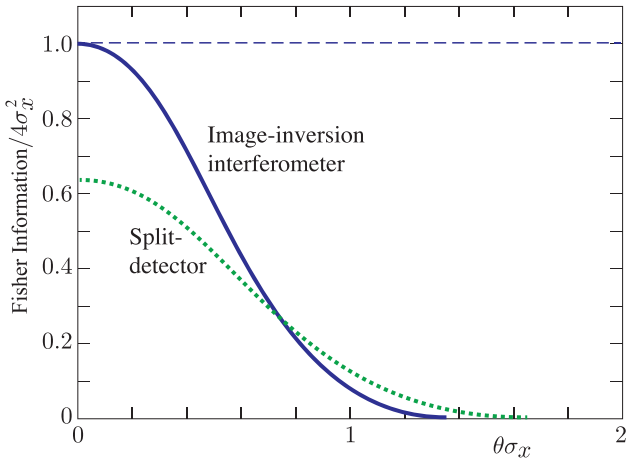

FIG. 1. Fisher information for estimation of the phase gradient θ using an optical beam of width σ_x in a single-photon state by use of a split-detector configuration (green dotted line) and an image-inversion (II) interferometer (solid blue line). For the II interferometer, the Fisher information reaches the quantum Fisher information (dashed lines) as $\theta \to 0$ (dashed line), while it is smaller by a factor $2/\pi$ for a configuration using a split detector in a lens' focal plane. The single-photon state corresponds to the maximum sensitivity of any classical illumination.

and the power difference $P_+ - P_-$ can be used to infer the displacement s. For a monochromatic Gaussian beam $\psi_0(x)$ with modulus $|\psi_0(x)|^2 = (1/\sqrt{2\pi}\sigma_x)\exp(-x^2/2\sigma_x^2)$ modulated by a linear phase factor $e^{-i\theta x}$, a lens of focal length f produces in the focal plane a Gaussian field $\psi_f(x)$ of width $\sigma_f = \lambda f/(4\pi\sigma_x)$ offset from the center by a distance $s_\theta = (\lambda f/2\pi)\theta$, where λ is the wavelength. The apparatus used for measurement of beam displacement s can therefore be readily adapted to measurement of the beam tilt θ. The Fisher information (FI) for such an arrangement is

$$F_{\rm SD}^{(1)}(\theta) = \frac{8}{\pi}\sigma_x^2/\xi(\theta\sigma_x), \tag{13}$$

where $\xi(y) = e^{4y^2}[1 - \mathrm{erf}^2(\sqrt{2}y)]$ and $\mathrm{erf}(y)$ is the error function. As illustrated in Fig. 1, $F_{\rm SD}^{(1)}(\theta)$ is a monotonic decreasing function of $\theta\sigma_x$, It has its maximum value of $\frac{8}{\pi}\sigma_x^2$ for $\theta\sigma_x \ll \frac{1}{2}$ (or $s_\theta \ll \sigma_f$). This is a factor of $\pi/2$ smaller than the standard quantum limit $F_Q^{(1)}(\theta) = 4\sigma_x^2$, corresponding to a sensitivity lower by a factor of $\sqrt{\pi/2} \approx 1.25$, as also noted in Ref. [25].

This shortfall of the split detector, which is applicable to the single-photon state (and hence the coherent state), also extends to other implementations aimed at surpassing the classical estimation limit by use of other nonclassical states [24,31]. For example, for light in a squeezed state with optimal mean photon number N, the FI is $\frac{8}{\pi}\sigma_x^2 N^{3/2}$, as compared to the quantum Fisher information $4\sigma_x^2 N^2$ for the maximally entangled N-photon state [cf. Eq. (9)].

B. Image-inversion interferometer

In the image-inversion interferometer, the beam modulated by the phase object is interrogated by an interferometer with an image inversion element (i.e., a mirror) in one arm, as illustrated conceptually in Fig. 2 [29,32]. For an optical beam of amplitude $\psi_0(x)$ and width σ_x, the beam transmitted through (or reflected from) the phase object has an amplitude $\psi(x) = \psi_0(x)e^{i\theta x}$, which is mixed with an inverted copy of itself $\psi(-x)$ to generate amplitudes $\frac{1}{2}[\psi(x) \pm \psi(-x)]$ at the output ports of the interferometer. The interferometer can be made using spatially separated paths, as depicted in Fig. 2 or implemented in another ancillary binary degree of freedom such as polarization [26,29,33,34]. The corresponding intensities $I_\pm(x) = \frac{1}{2}|\psi(x) \pm \psi(-x)|^2$ are measured with two detectors of areas greater than the beam cross section σ_x. The result is the two signals $P_\pm = \frac{1}{2} \pm \frac{1}{2}\,\mathrm{Re}\int dx\, \psi_0^*(x)\psi_0(-x)e^{i2\theta x}$, where we have assumed that $\int |\psi_0(x)|^2 dx = 1$. In essence, this binary measurement represents projections of the spatial distribution onto its even (+) and odd (−) components. If $\psi_0(x)$ is an even function, then

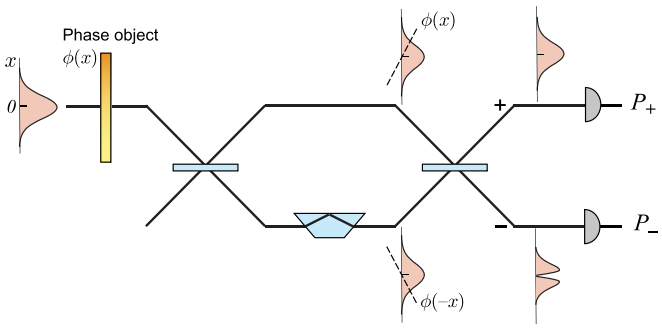

FIG. 2. Measurement of the optical phase gradient by use of an image-inversion interferometer.

$$P_+ = \int dx\, |\psi_0(x)|^2 \cos^2(\theta x),$$
$$P_- = \int dx\, |\psi_0(x)|^2 \sin^2(\theta x). \tag{14}$$

For a Gaussian function, the modulus $|\psi_0(x)|^2 = (1/\sqrt{2\pi}\sigma_x)\exp(-x^2/2\sigma_x^2)$,

$$P_\pm = \tfrac{1}{2}\left(1 \pm e^{-2\theta^2\sigma_x^2}\right), \tag{15}$$

and the difference $P_+ - P_- = \exp(-2\theta^2\sigma_x^2)$ is a monotonic decreasing function of $\theta\sigma_x$ that can be readily used to calculate the phase gradient θ.

Single-photon Fisher information. If the probe wave is in a single-photon state, then the above classical analysis is applicable with the signals P_+ and P_- interpreted as the probabilities of the photon being detected in the + and − output ports, respectively. The FI associated with such measurement is

$$F^{(1)}(\theta) = \frac{1}{P_+}\left(\frac{dP_+}{d\theta}\right)^2 + \frac{1}{P_-}\left(\frac{dP_-}{d\theta}\right)^2. \tag{16}$$

Using the expressions in (15), it follows that the FI is

$$F^{(1)}(\theta) = 4\sigma_x^2 \,/\, \zeta^2(\theta\sigma_x), \tag{17}$$

where $\zeta^2(y) = [\exp(4y^2) - 1]/4y^2$ is a monotonically increasing function of y with value equal to 1 for $y = 0$ and ≈ 1.7 for $y = \frac{1}{2}$. Therefore, in the limit $\theta\sigma_x \ll 1$, i.e., when the phase varies slowly within the beam width, the factor

$\zeta(\sigma_x\theta) = 1$, so that $F^{(1)}(\theta) = F_Q^{(1)}(\theta)$, i.e., the II interferometer provides the best possible precision for estimating θ. For a fixed value of σ_x, as θ increases, $F^{(1)}(\theta)$ drops as depicted in Fig. 1, reaching one-half of its maximum value at $\theta \approx 0.56/\sigma_x$, so that the larger the beam width is, the faster $F^{(1)}(\theta)$ drops as a function of θ. Based on Eq. (17), for a given value of θ, the FI as a function of σ_x rises to a peak value at $\sigma_x \approx 0.632/\theta$ and drops with further increase of σ_x. The Cramér-Rao estimation error σ_θ corresponding to $F^{(1)}(\theta)$ satisfies the relation

$$\sigma_x\sigma_\theta = \tfrac{1}{2}\,\zeta(\theta\sigma_x) \tag{18}$$

so that it rises above the minimum value of $1/2$ as θ increases.

The FI for the II interferometer and the split detector are compared in Fig. 1. For small θ the II interferometer is superior to the split detector by the largest factor, but this advantage diminishes as θ increases, and the split detector becomes slightly more sensitive for $\theta > 0.74/\sigma_x$.

N-photon Fisher information. A generalized image-inversion interferometer acting on a phase modulated optical beam in the maximally entangled N-photon state in Eq. (8) is conceptualized to operate in three stages. In the first, the state is converted into a generalized NOON state in the basis of the two orthogonal modes of the interferometer $|+\rangle$ and $|-\rangle$ (e.g., the upper and lower paths):

$$|\psi_1\rangle = \int dx f_0(x) e^{-iN\theta x} \frac{1}{\sqrt{2}}[|+,x\rangle^{\otimes N}|-,x\rangle^{\otimes 0} + |+,x\rangle^{\otimes 0}|-,x\rangle^{\otimes N}]. \tag{19}$$

In the second stage, spatial inversion is introduced in the $|-\rangle$ mode, generating the state

$$|\psi_2\rangle = \int dx f_0(x) \frac{1}{\sqrt{2}}[e^{-iN\theta x}|+,x\rangle^{\otimes N}|-,x\rangle^{\otimes 0} + e^{iN\theta x}|+,x\rangle^{\otimes 0}|-,x\rangle^{\otimes N}], \tag{20}$$

where $f_0(x)$ was assumed to be an even function. In the third stage, the $|+\rangle$ and $|-\rangle$ modes are recombined at a beam splitter and the photon-number parity is measured at either output port [17,35–38], a measurement represented by the observable operator

$$\Pi = i^N \sum_{k=0}^{N} (-1)^k |k, N-k\rangle\langle N-k, k|. \tag{21}$$

The result of a parity measurement is $+1$ if the photon number detected in the measured mode is even, and -1 if it is odd, and the associated probabilities are P_+ and P_-, with $P_+ + P_- = 1$ and $P_+ - P_- = \langle\Pi\rangle$, following the standard approach for parity measurement [35]. Based on Eq. (16), the Fisher information can be expressed in terms of $\langle\Pi\rangle$ as

$$F^{(N)}(\theta) = \frac{\left|\frac{d\langle\Pi\rangle}{d\theta}\right|^2}{1 - \langle\Pi\rangle^2}. \tag{22}$$

To determine an expression of $\langle\Pi\rangle = \langle\psi_2|\Pi|\psi_2\rangle$ for the NOON state in (20) in terms of θ we note that the only terms in the expression (21) of Π that contribute to $\langle\Pi\rangle$ are $k = 0$ and $k = N$, and assuming that N is even,

$$\langle\Pi\rangle = \int dx |f_0(x)|^2 \cos(N\theta x). \tag{23}$$

Assuming a Gaussian function,

$$F^{(N)}(\theta) = 4N^2\sigma_x^2/\zeta^2(N\theta\sigma_x) = F_Q^{(N)}/\zeta^2(N\theta\sigma_x), \tag{24}$$

where, as before, $\zeta^2(y) = [\exp(4y^2) - 1]/4y^2$. Thus, in the limit $\theta\sigma_x \to 0$, $F^{(N)}(\theta) = F_Q^{(N)}$, i.e., the quantum Fisher information is attained at small phase-gradient beam-width product.

Based on Eqs. (24) and (17), it follows that

$$F^{(N)}(\theta) = N^2 F^{(1)}(N\theta). \tag{25}$$

Hence, in comparison with the single-photon case, the maximum achievable Fisher information is greater by a factor of N^2, but drops from its maximal value with increase of $\theta\sigma_x$ at a rate N times greater. This remarkable scaling relation, illustrated in Fig. 3, highlights both the precision enhancing power of the quantum advantage and its vulnerability to large beam width or aperture area.

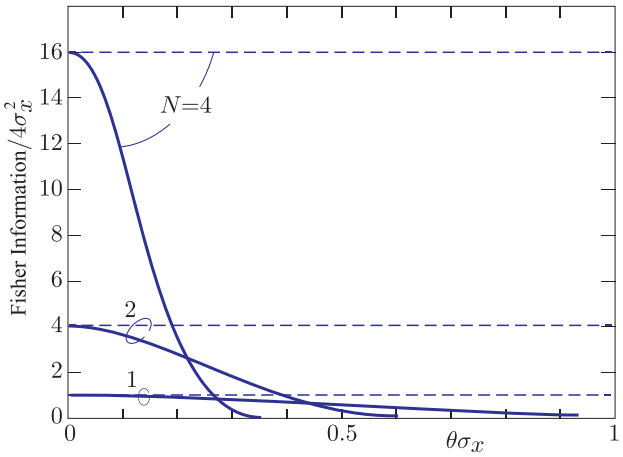

FIG. 3. Fisher information for estimation of the phase gradient θ using an optical beam of width σ_x in a state with $N = 1, 2, 4$ photons, assuming measurements with an image inversion interferometer. In each case, the Fisher information reaches the quantum Fisher information (dashed lines) as $\theta\sigma_x \to 0$ (dashed lines).

Implementation of the II interferometer for an arbitrary N-photon state requires replacing the first beam splitter with a device that generates the generalized NOON state $|\psi_1\rangle$ in Eq. (19) from the state $|\psi\rangle$ in Eq. (8). This may be accomplished by use of a wavefront-division component as depicted in Fig. 4. Here, the phase-modulated beam in the state $|\psi\rangle$ of Eq. (8) is split into two spatial modes: the positive spatial mode, which has all N photons in the region $x > 0$, and the negative spatial mode, which has all N photons in the $x < 0$ region. These modes are directed to the two arms of the interferometer (using, e.g., prisms or a spatial light modulator) so that the state is $|\psi_1\rangle$. After image inversion, the negative mode is converted into a positive mode, but with phase $\phi(-x)$, so that the phase difference between the modes becomes $\phi(x) - \phi(-x) = \theta x$. After recombination at the second beam splitter, by measuring the parity of the detected photons, the sensitivity described by Eq. (25) is achieved.

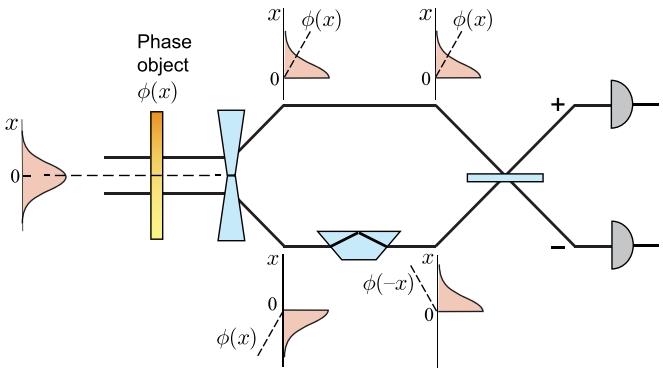

FIG. 4. Wavefront-division image-inversion interferometer generating the generalized NOON state. The detectors measure photon-number parity.

While methods for creating the N-photon spatial entanglement required is an ongoing field of research, for $N = 2$ the state may be readily created by use of a process of collinear downconversion, which exhibits a high degree of spatial entanglement [39]. We expect that higher-order and cascaded nonlinearities will similarly be able to create the characteristic entanglement needed for for N-photon protocol. Also, for $N = 2$, the parity of the photon number may be readily determined by use of a coincidence circuit. The II interferometer itself may also be implemented in polarization modes [26], rather than spatially separated path modes.

IV. CONCLUSION

We have shown that, for a single-photon quantum state, the ultimate quantum bound on the precision of estimates of the phase gradient introduced by an optical element probed by a beam of finite width (or estimates of the tilt of an optical wavefront within a finite aperture) reproduces the Fourier-transform uncertainty principle. For an N-photon quantum state that is maximally entangled in the spatial domain, the quantum precision bound is superior by the familiar factor of N and the uncertainty product is tighter by the same factor. Here, uncertainty is defined as a bound on the statistical accuracy—as dictated by the quantum Fisher information—of estimating the phase gradient, which corresponds to the transverse component of the optical field's wave vector.

We have determined the sensitivity of a specific optical configuration for measurement of the phase gradient, namely the image-inversion (II) interferometer, and shown that it meets the standard quantum limit for small phase-gradient beam-width product and a single-photon state (or a coherent state). It also attains the Heisenberg quantum precision limit for an N-photon quantum state with maximum spatial entanglement. The II interferometer achieves this supersensitivity by utilizing interference between the phase-modulated beam and a spatially inverted copy of itself, along with binary projective measurements similar to those used in other recent applications [27,40–42]. For the N-photon state the system is a NOON-like interferometer. Unfortunately, the precision drops rapidly as the phase-gradient beam-width product increases, and the rate of such drop is greater for larger N. This is another manifestation of the fragility of quantum supersensitivity. While the regime of small beam width, which is desirable since it enables greater spatial resolution in scanning systems, preserves the quantum advantage, it corresponds to lower quantum sensitivity since the QFI is proportional to the squared beam width. An optimal beam width is inversely proportional to the phase gradient.

In comparison with a measurement configuration using a split detector placed in the focal plane of a Fourier-transform imaging system, the sensitivity of the II interferometer is superior by a factor of at least $\sqrt{\pi/2} \approx 1.25$ for the single-photon state. Other nonclassical states have been considered for use with the split-detector configuration, but their sensitivity is also limited by the same factor. The performance of the II interferometer is actually similar to that of a homodyne detection system designed to measure beam displacement by use of even and odd spatially distributed signal and local oscillator beams [24].

ACKNOWLEDGMENT

This work was supported in part by Air Force Research Laboratory Grant No. FA8651-19-2-0001.

[1] L. Mandel and E. Wolf, *Optical Coherence and Quantum Optics* (Cambridge University, New York, 1995), Vol. 64, p. 1192.
[2] C. M. Caves, Quantum-mechanical noise in an interferometer, Phys. Rev. D **23**, 1693 (1981).
[3] S. L. Braunstein, How large a sample is needed for the maximum likelihood estimator to be approximately Gaussian? J. Phys. A **25**, 3813 (1992).
[4] M. J. Holland and K. Burnett, Interferometric Detection of Optical Phase Shifts at the Heisenberg Limit, Phys. Rev. Lett. **71**, 1355 (1993).
[5] D. S. Simon, Quantum sensors: Improved optical measurement via specialized quantum states, J. Sens. **2016**, 6051286 (2016).
[6] V. Giovannetti, S. Lloyd, and L. Maccone, Quantum-enhanced measurements: Beating the standard quantum limit, Science **306**, 1330 (2004).
[7] C. W. Helstrom, *Quantum Detection and Estimation Theory* (Academic Press, London, 1976).
[8] A. Holevo, *Probabilistic and Statistical Aspects of Quantum Mechanics* (North-Holland, Amsterdam, 1982).
[9] S. L. Braunstein and C. M. Caves, Statistical Distance and the Geometry of Quantum States, Phys. Rev. Lett. **72**, 3439 (1994).
[10] V. Giovannetti, S. Lloyd, and L. Maccone, Advances in quantum metrology, Nature Photonics **5**, 222 (2011).
[11] V. Giovannetti, S. Lloyd, and L. Maccone, Quantum Metrology, Phys. Rev. Lett. **96**, 010401 (2006).

[12] K. Matsumoto, A new approach to the Cramer - Rao-type bound of the pure-state model, J. Phys. A **35**, 3111 (2002).
[13] R. Demkowicz-Dobrzański, J. Kołodyński, and M. Gută, The elusive Heisenberg limit in quantum-enhanced metrology, Nature Commun. **3**, 1063 (2012).
[14] L.-L. Sun, Y.-S. Song, C.-F. Qiao, S. Yu, and Z.-B. Chen, Uncertainty relation based on unbiased parameter estimations, Phys. Rev. A **95**, 022112 (2017).
[15] S. L. Braunstein, C. M. Caves, and G. J. Milburn, Generalized uncertainty relations: Theory, examples, and Lorentz invariance, Ann. Phys. **247**, 135 (1996).
[16] H. Shin, K. W. C. Chan, H. J. Chang, and R. W. Boyd, Quantum Spatial Superresolution by Optical Centroid Measurements, Phys. Rev. Lett. **107**, 083603 (2011).
[17] G. R. Jin, W. Yang, and C. P. Sun, Quantum-enhanced microscopy with binary-outcome photon counting, Phys. Rev, A **95**, 013835 (2017).
[18] J. P. Dowling, Quantum optical metrology - the lowdown on high-N00N states, Contemp. Phys. **49**, 125 (2008).
[19] H. Lee, P. Kok, C. P. Williams, and J. P. Dowling, From linear optical quantum computing to Heisenberg-limited interferometry, J. Opt. B: Quantum Semiclass. Opt. **6**, S796 (2004).
[20] D. Strekalov and J. P. Dowling, Two-photon interferometry for high-resolution imaging, J. Mod. Opt. **49**, 519 (2002).
[21] U. Dorner, R. Demkowicz-Dobrzanski, B. J. Smith, J. S. Lundeen, W. Wasilewski, K. Banaszek, and I. A. Walmsley, Optimal Quantum Phase Estimation, Phys. Rev. Lett. **102**, 040403 (2009).
[22] J. W. Goodman, *Introduction to Fourier Optics*, 3rd ed. (Roberts & Company, Greenwrood Village, 2005).
[23] R. K. Tyson, *Principles of Adaptive Optics, Fourth Edition*, 4th ed. (Taylor & Francis, Boca Raton, 2015).
[24] M. T. L. Hsu, V. Delaubert, P. K. Lam, and W. P. Bowen, Optimal optical measurement of small displacements, J. Opt. B: Quantum Semiclass. Opt. **6**, 495 (2004).
[25] S. M. Barnett, C. Fabre, and A. Maître, Ultimate quantum limits for resolution of beam displacements, Eur. Phys. J. D **22**, 513 (2003).
[26] W. Larson, N. V. Tabiryan, and B. E. A. Saleh, A common-path polarization-based image-inversion interferometer, Opt. Express **27**, 5685 (2019).
[27] Z. S. Tang, K. Durak, and A. Ling, Fault-tolerant and finite-error localization for point emitters within the diffraction limit, Opt. Express **24**, 22004 (2016).
[28] L. Cohen, D. Istrati, L. Dovrat, and H. S. Eisenberg, Super-resolved phase measurements at the shot noise limit by parity measurement, Opt. Express **22**, 11945 (2014).
[29] D. Weigel, A. Kiessling, and R. Kowarschik, Aberration correction in coherence imaging microscopy using an image inverting interferometer, Opt. Express **23**, 20505 (2015).
[30] R. Demkowicz-Dobrzański, M. Jarzyna, and J. Kołodyński, Quantum limits in optical interferometry, Prog. Opt. **60**, 345 (2015).
[31] N. Treps, N. Grosse, W. P. Bowen, and C. Fabre, A Quantum Laser Pointer, Science **301**, 940 (2003).
[32] D. Weigel, H. Babovsky, A. Kiessling, and R. Kowarschik, Widefield microscopy with infinite depth of field and enhanced lateral resolution based on an image inverting interferometer, Opt. Commun. **342**, 102 (2015).
[33] A. Aiello, F. Töppel, C. Marquardt, E. Giacobino, and G. Leuchs, Quantum-like nonseparable structures in optical beams, New J. Phys. **17**, 17 043024 (2015).
[34] R. Nair and M. Tsang, Interferometric superlocalization of two incoherent optical point sources, Opt. Express **24**, 3684 (2016).
[35] K. P. Seshadreesan, S. Kim, J. P. Dowling, and H. Lee, Phase estimation at the quantum Cramér-Rao bound via parity detection, Phys. Rev. A **87**, 043833 (2013).
[36] Y. Ben-Aryeh, Phase estimation by photon counting measurements in the output of a linear Mach - Zehnder interferometer, J. Opt. Soc. Am. B **29**, 2754 (2012).
[37] W. Zhong, Y. Huang, X. Wang, and S.-L. Zhu, Optimal conventional measurements for quantum-enhanced interferometry, Phys. Rev. A **95**, 052304 (2017).
[38] M. D. Vidrighin, G. Donati, M. G. Genoni, X. M. Jin, W. S. Kolthammer, M. S. Kim, A. Datta, M. Barbieri, and I. A. Walmsley, Joint estimation of phase and phase diffusion for quantum metrology, Nature Commun. **5**, 3532 (2014).
[39] J. Schneeloch and J. C. Howell, Introduction to the transverse spatial correlations in spontaneous parametric down-conversion through the biphoton birth zone, J. Opt. **18**, 053501 (2016).
[40] W. K. Tham, H. Ferretti, and A. M. Steinberg, Beating Rayleigh's Curse by Imaging Using Phase Information, Phys. Rev. Lett. **118**, 070801 (2017).
[41] M. Tsang, R. Nair, and X.-M. Lu, Quantum Theory of Superresolution for Two Incoherent Optical Point Sources, Phys. Rev. X **6**, 031033 (2016).
[42] M. Paúr, B. Stoklasa, Z. Hradil, L. L. Sánchez-Soto, and J. Rehacek, Achieving the ultimate optical resolution, Optica **3**, 1144 (2016).